

Supporting Information for:

# *In Situ* Assembly of Octahedral Fe(II) Complexes for the Enantiomeric Excess Determination of Chiral Amines Using CD Spectroscopy

Justin Dragna, Gennaro Pescitelli, Lee Tran, Vincent M. Lynch, Eric V. Anslyn,\* and Lorenzo Di Bari\*

I. General Experimental Details

II. Experimental Details on:

- a) Calibration Curves and Test Sample Experimental for **MBI**
- b) Calibration Curves and Test Sample Experimental for **CEI**
- c) Calibration Curves and Test Sample Experimental for **HPI**

III. Calculations for:

- a) Probability
- b) CD curves in visible region

IV. Tables

Table S-1. A summary of the calculated probabilities for populations of different isomer sets and how they vary with *ee*.

Table S-2. A summary of the calculated probabilities for populations of different isomer sets at different *ees*

V. Figures

Figure S-1. Overlay of all data points for the calibration curves developed for **MBI** at 3mM, 4mM, and 5mM at 1mM Fe(TfO)<sub>2</sub> in acetonitrile in a 0.1cm quartz cuvette.

Figure S-2. Overlay of all data points for calibration curves developed for **MBI** at 6mM, 7mM, 8mM, and 9mM at 1mM Fe(TfO)<sub>2</sub> in acetonitrile in a 0.1cm quartz cell.

Figure S-3. Overlay of all data points for calibration curve developed for **MBI** at 6mM and 1mM Fe(TfO)<sub>2</sub> in acetonitrile in a 0.1cm quartz cell.

Figure S-4. A graph of the probability of the four different isomer sets as functions of enantiomeric excess.

Figure S-5. A graph of the four different isomer sets as a functions of enantiomeric excess with the introduction of a sign change for predominantly *S* isomer sets.

Figure S-6. The <sup>1</sup>H NMR of the **MBI**-iron(II) complex at -100% *ee*.

Figure S-7. The <sup>1</sup>H NMR of the **MBI**-iron(II) complex at -60% *ee*.

Figure S-8. The <sup>1</sup>H NMR of the **MBI**-iron(II) complex at -20% *ee*.

Figure S-9. The <sup>1</sup>H NMR of the **MBI**-iron(II) complex at 0% *ee*.

Figure S-10. The <sup>1</sup>H NMR of the **MBI**-iron(II) complex at 20% *ee*.

Figure S-11. The <sup>1</sup>H NMR of the **MBI**-iron(II) complex at 60% *ee*.

Figure S-12. The <sup>1</sup>H NMR of the **MBI**-iron(II) complex at 100% *ee*.

Figure S-13. <sup>1</sup>H NMR of 10mM aldehyde **3** and 6mM **MBI**.

Figure S-14. <sup>1</sup>H NMR of 10mM aldehyde **3** and 6mM of **CEI**.

Figure S-15. <sup>1</sup>H NMR of 10mM aldehyde **3** and 6mM **HPI**.

## VI. X-ray Crystallographic Data

Table S-3. Crystallographic data.

Table S-4. Fractional coordinates and equivalent isotropic thermal parameters (Å<sup>2</sup>) for the non-hydrogen atoms.

Table S-5. Bond Lengths (Å) and angles (°) for the non-hydrogen atoms.

Table S-6. Anisotropic thermal parameters for the non-hydrogen atoms.

Table S-7. Fractional coordinates and isotropic thermal parameters (Å<sup>2</sup>) for the hydrogen atoms.

## VII. Computational Details

### I. General Experimental Details:

All reagents were purchased from commercial sources and used as received with the exception of aldehyde **1**. Aldehyde **1** was purified by sublimation under high vacuum with mild heat (60-70°C) using a cold finger apparatus before use in the assay. HPLC grade acetonitrile purged for 2 hours with nitrogen was used throughout. An automated Varian Mercury 400MHz spectrometer was used to collect <sup>1</sup>H NMR spectra. Solutions were dispensed into Microamp<sup>®</sup>

optical 96-well reaction plates purchased from applied biosystems using multichannel and single channel eppendorf research pipettes. CD spectra measurements were taken on a JASCO-815 CD spectrometer outfitted with an autosampler. 96-well reaction plates were sealed during equilibration periods using viewseal advanced sealing tapes purchased from E&K Scientific.

## **II. Experimental Details on:**

### a) Calibration Curves and Test Sample Experimental for **MBI**:

A solution of aldehyde **1** at 18mM was transferred in 100 microL aliquots to a 96-well plate. To this was added 100 microL aliquots of a solution of 15mM 1-aminomethyl benzene for the calibration curve developed at 5mM, 12mM 1-aminomethylbenzene for calibration curve developed at 4mM, and 9mM for the calibration curve developed at 3mM. 100microL of a 3mM Fe(TfO)<sub>2</sub> solution was then aliquoted into each well and the plate was sealed for 3 hours before being placed on the autosampler for spectral measurements. Test samples were prepared and run in an analogous manner from a 15mM stock solution of 1-aminomethylbenzene and diluted accordingly.

### b) Calibration Curves and Test Sample Experimental for **CEI**:

A solution of aldehyde **1** at 36mM was transferred in 100 microL aliquots to a 96-well plate. To this was added 100 microL aliquots of a solution of 27mM 1-cyclohexylethyl amine for the calibration curve developed at 9mM, 24mM 1-cyclohexylethyl amine for the calibration curve developed at 8mM, 21mM for the calibration curve developed at 7mM and 18mM for the calibration curve developed at 6mM. 100microL of a 3mM Fe(TfO)<sub>2</sub> solution was then aliquoted into each well and the plate was sealed for 3 hours before being placed on the autosampler for spectral measurements. Test samples were prepared in an analogous manner from a 36mM stock solution of 1-cyclohexylethyl amine and diluted accordingly.

### c) Calibration Curves and Test Sample Experimental for **HPI**:

A solution of aldehyde **1** at 18mM was transferred in 100 microL aliquots to a 96-well plate. To this was added 100 microL aliquots of a solution of 18mM 2-aminoheptane for the

calibration curve developed at 6mM. 100microL of a 3mM Fe(TfO)<sub>2</sub> solution was then aliquoted into each well and the plate was sealed for 3 hours before being placed on the autosampler for spectral measurements. Test samples were prepared in an analogous manner from a 36mM stock solution of 2-aminoheptane and diluted accordingly.

### III. Calculations for:

a) Probability:

The probability (P) is calculated for a pool of 100 molecules.

#### **100% ee**

Isomer set (R,R,R)

$$P = \left(\frac{100}{100}\right)\left(\frac{99}{99}\right)\left(\frac{98}{98}\right) = 1$$

Because the sum of the probabilities must equal 1 isomer sets (R,R,S), (S,S,R), and (S,S,S) must equal 0.

#### **80% ee**

**At 80% ee there are 90 imine molecules with R stereogenic centers and 10 imine molecules with S stereogenic centers.**

Isomer set (R,R,R)

$$P = \left(\frac{90}{100}\right)\left(\frac{89}{99}\right)\left(\frac{88}{98}\right) = 0.73$$

Isomer set (R,R,S)

$$P = 3 \left(\frac{90}{100}\right)\left(\frac{89}{99}\right)\left(\frac{10}{98}\right) = 0.25$$

Isomer set (S,S,R)

$$P = 3 \left(\frac{10}{100}\right)\left(\frac{9}{99}\right)\left(\frac{90}{98}\right) = 0.0083$$

Isomer set (*S,S,S*)

$$P = \left(\frac{10}{100}\right)\left(\frac{9}{99}\right)\left(\frac{8}{98}\right) = 0.00074$$

The probabilities for the remaining *ees* are calculated in an analogous manner, and are summarized in Table S-1. A graph of the probabilities for the different isomer sets is shown in Figure S-4.

Enantiomers have equal and opposite CD signals. In order to reflect this in the probabilistic model, a negative sign is introduced for isomer sets that are predominantly *S* as seen in Table S-2. This is based on the sign of CD signal observed for -100% *ee* (all *S* imines) at the wavelength the calibration curves were taken at. A graph of how the probabilities vary with *ee* for the various isomer sets is shown in Figure S-5.

Finally, the observed CD signal will result in cancellation from enantiomeric pairs between predominantly *R* and predominantly *S* isomer sets. This can be reflected by summing the signed probabilities from Table S-2. The arithmetic sums are in Table 2. and a graph of the arithmetic sums are in Figure 4.

#### b) CD curves in visible region

In the visible region, the calculations also led to a bisignate CD feature, though with opposite sign with respect to the experiment as far as the  $\Delta$ -*fac* diastereomer is concerned (not shown). The discrepancy was not alleviated after considering the contributions from other diastereomers. For our purposes, is interesting to notice that population and orbital analysis revealed that the two calculated CD bands between 500-700 nm are both due to the combination of d-to- $\pi^*$  transitions involving the two lowest-energy and degenerate d $\pi$  orbitals. Moreover, both transitions have the same E symmetry, therefore they cannot represent two ECCD components.

**IV. Tables:**

<i>ee</i>	( <i>R,R,R</i> )	( <i>R,R,S</i> )	( <i>S,S,R</i> )	( <i>S,S,S</i> )	sum
1	1	0	0	0	1
0.8	0.73	0.25	0.025	0.00074	1
0.6	0.51	0.39	0.094	0.0071	1
0.4	0.34	0.45	0.19	0.025	1
0.2	0.21	0.44	0.29	0.061	1
0	0.12	0.38	0.38	0.12	1
-0.2	0.061	0.29	0.44	0.21	1
-0.4	0.025	0.19	0.45	0.34	1
-0.6	0.0071	0.094	0.39	0.51	1
-0.8	0.00074	0.025	0.25	0.73	1
-1	0	0	0	1	1

Table S-1. A summary of the calculated probabilities for populations of different isomer sets and how they vary with *ee*. The last column shows that the sum of all the probabilities is always 1 as required for a probabilistic model.

<i>ee</i>	( <i>R,R,R</i> )	( <i>R,R,S</i> )	( <i>S,S,R</i> )	( <i>S,S,S</i> )
1	1	0	0	0
0.8	0.73	0.25	-0.025	-0.00074
0.6	0.51	0.39	-0.094	-0.0071
0.4	0.34	0.45	-0.19	-0.025
0.2	0.21	0.44	-0.29	-0.061
0	0.12	0.38	-0.38	-0.12
-0.2	0.061	0.29	-0.44	-0.21
-0.4	0.025	0.19	-0.45	-0.34
-0.6	0.0071	0.094	-0.39	-0.51
-0.8	0.00074	0.025	-0.25	-0.73
-1	0	0	0	-1

Table S-2. A summary of the calculated probabilities for populations of different isomer sets at different *ees*. A negative sign is introduced for the probabilities for (*S,S,R*) and (*S,S,S*) to reflect the equal and opposite nature of CD signals for different enantiomers.

V. Figures:

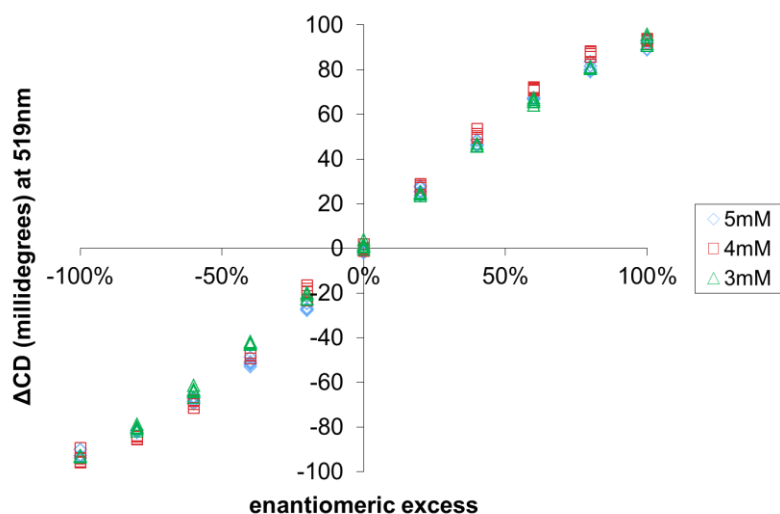


Figure S-1. Overlay of all data points for the calibration curves developed for **MBI** at 3mM, 4mM, and 5mM at 1mM Fe(TfO)<sub>2</sub> in acetonitrile in a 0.1cm quartz cuvette.

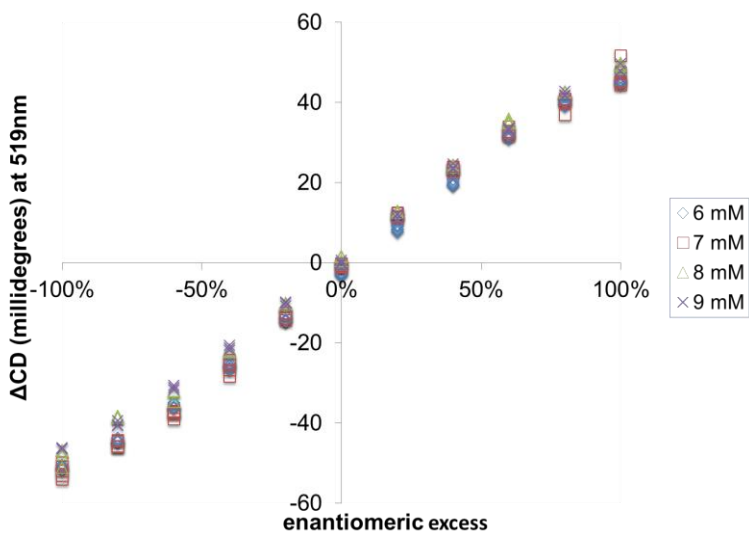


Figure S-2. Overlay of all data points for calibration curves developed for **CEI** at 6mM, 7mM, 8mM, and 9mM at 1mM Fe(TfO)<sub>2</sub> in acetonitrile in a 0.1cm quartz cell.

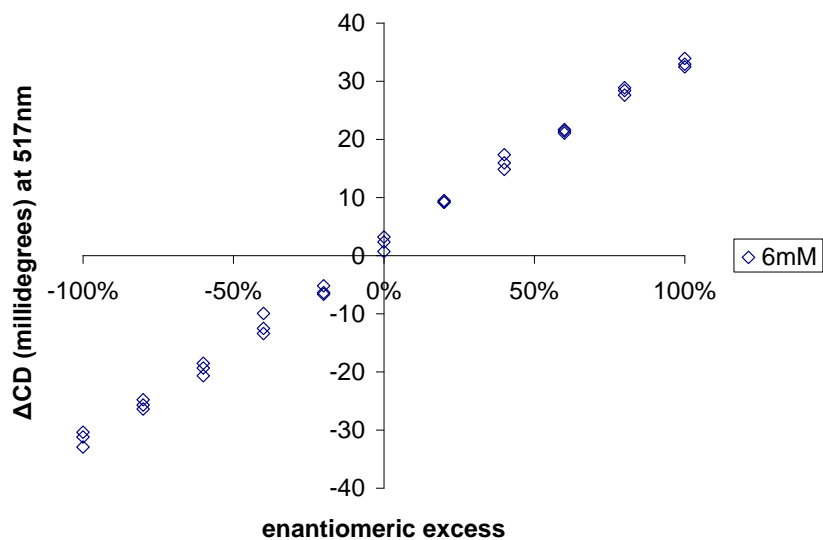


Figure S-3. Overlay of all data points for calibration curve developed for **HPI** at 6mM and 1mM Fe(TfO)<sub>2</sub> in acetonitrile in a 0.1cm quartz cell.

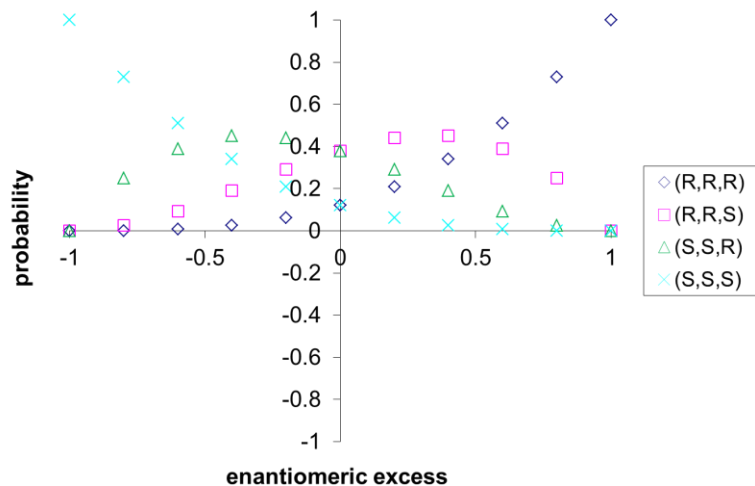


Figure S-4. A graph of the probability of the four different isomer sets as functions of enantiomeric excess.



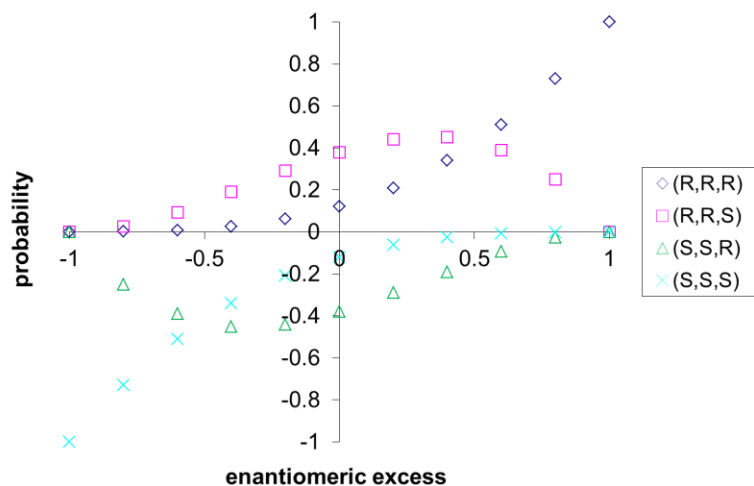


Figure S-5. A graph of the four different isomer sets as a functions of enantiomeric excess with the introduction of a sign change for predominantly *S* isomer sets.

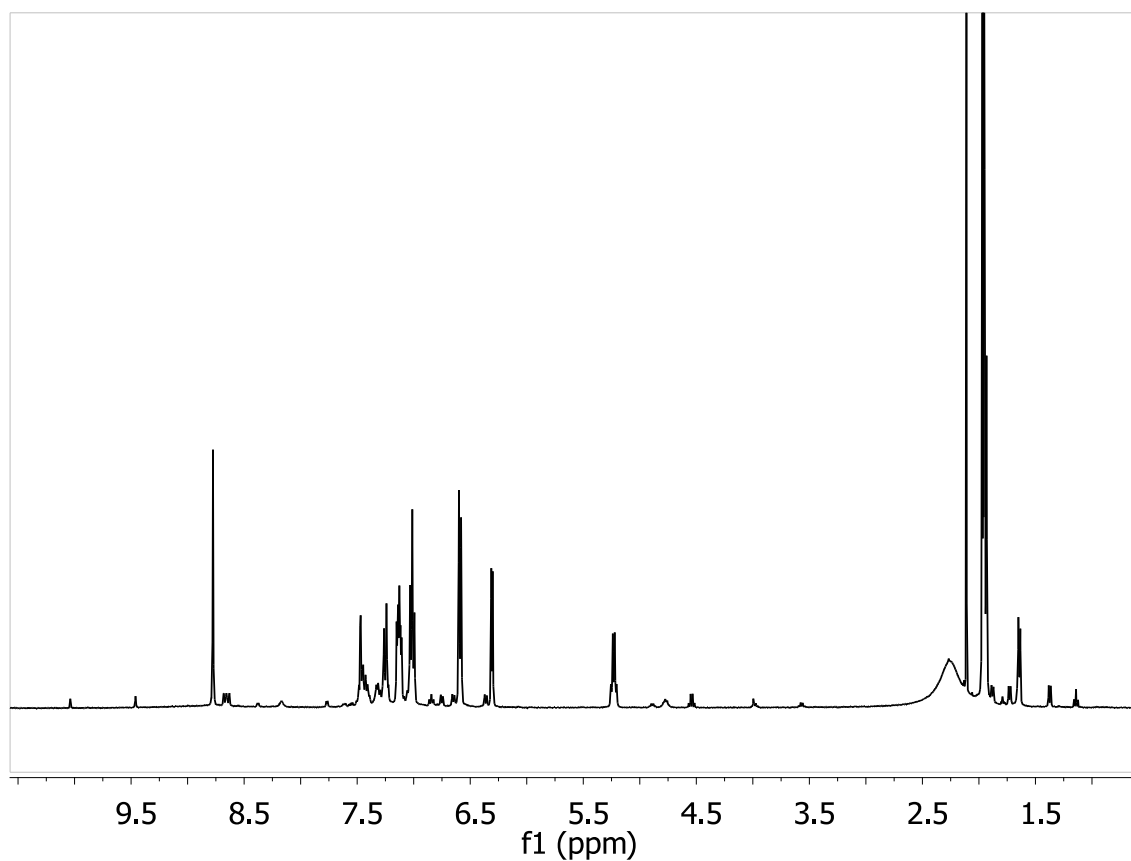
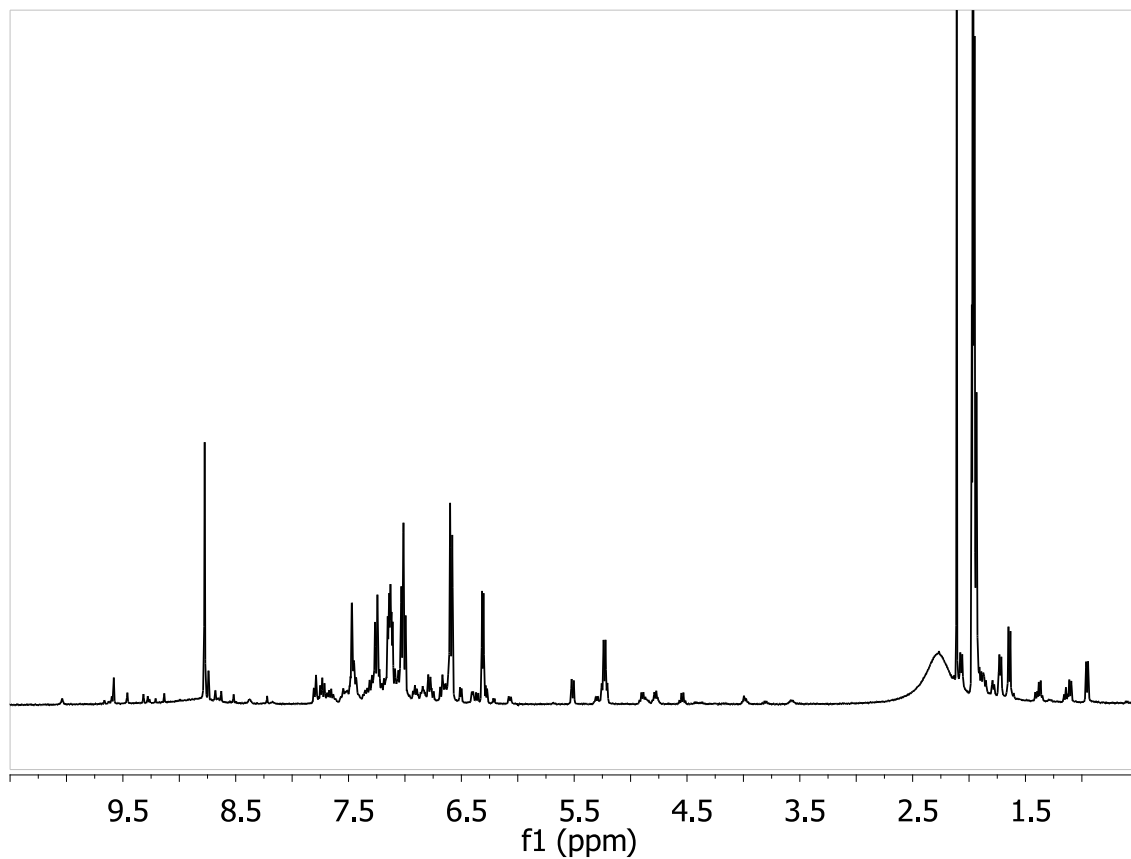


Figure S-6. The <sup>1</sup>H NMR of the **MBI**-iron(II) complex at -100% *ee*.



S-7. The  $^1\text{H}$  NMR of the **MBI**-iron(II) complex at -60% *ee*.

Figure

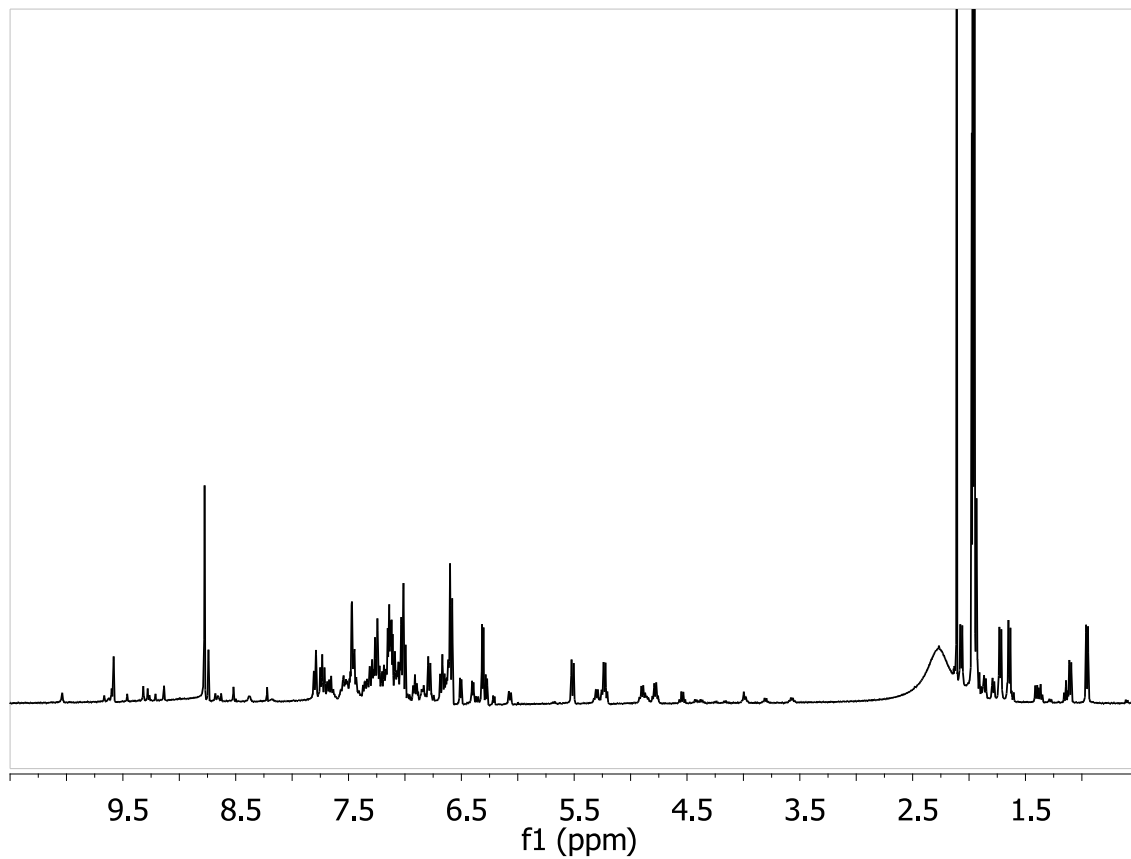


Figure S-8. The  $^1\text{H}$  NMR of the **MBI**-iron(II) complex at -20% *ee*.

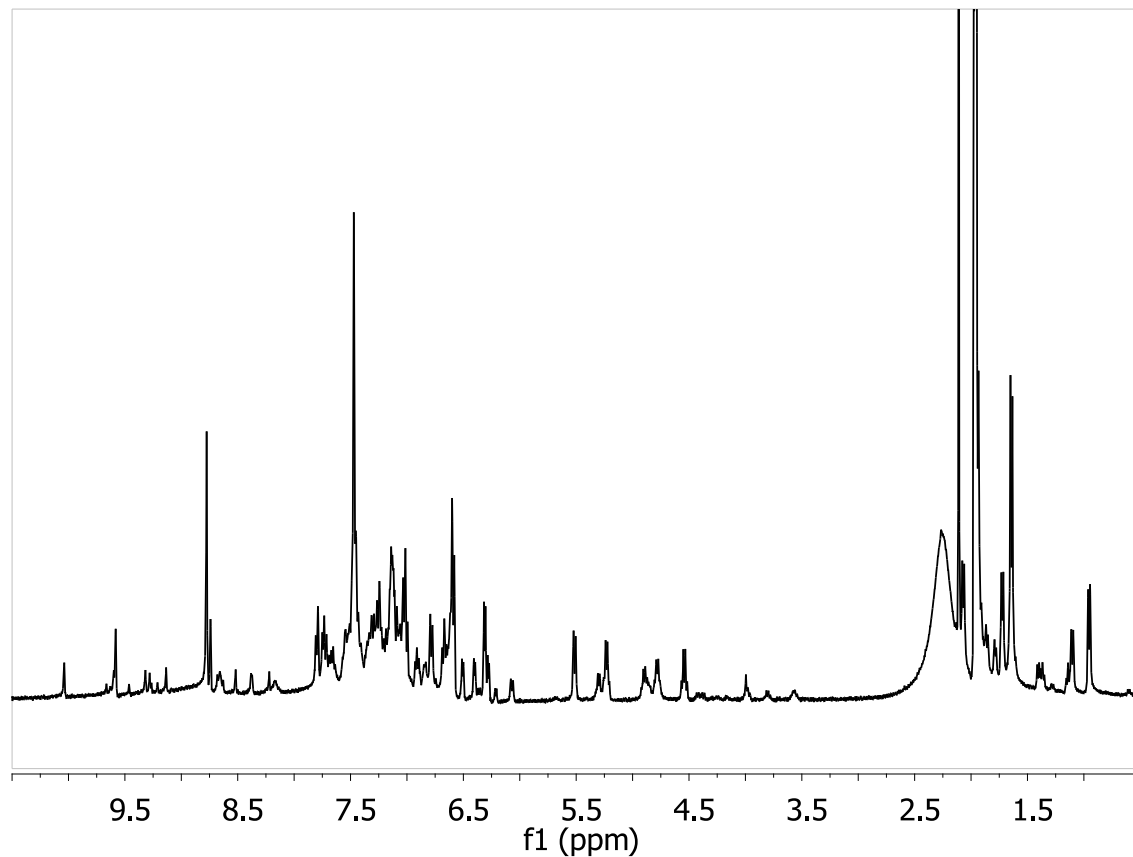


Figure S-9. The  $^1\text{H}$  NMR of the **MBI**-iron(II) complex at 0% *ee*.

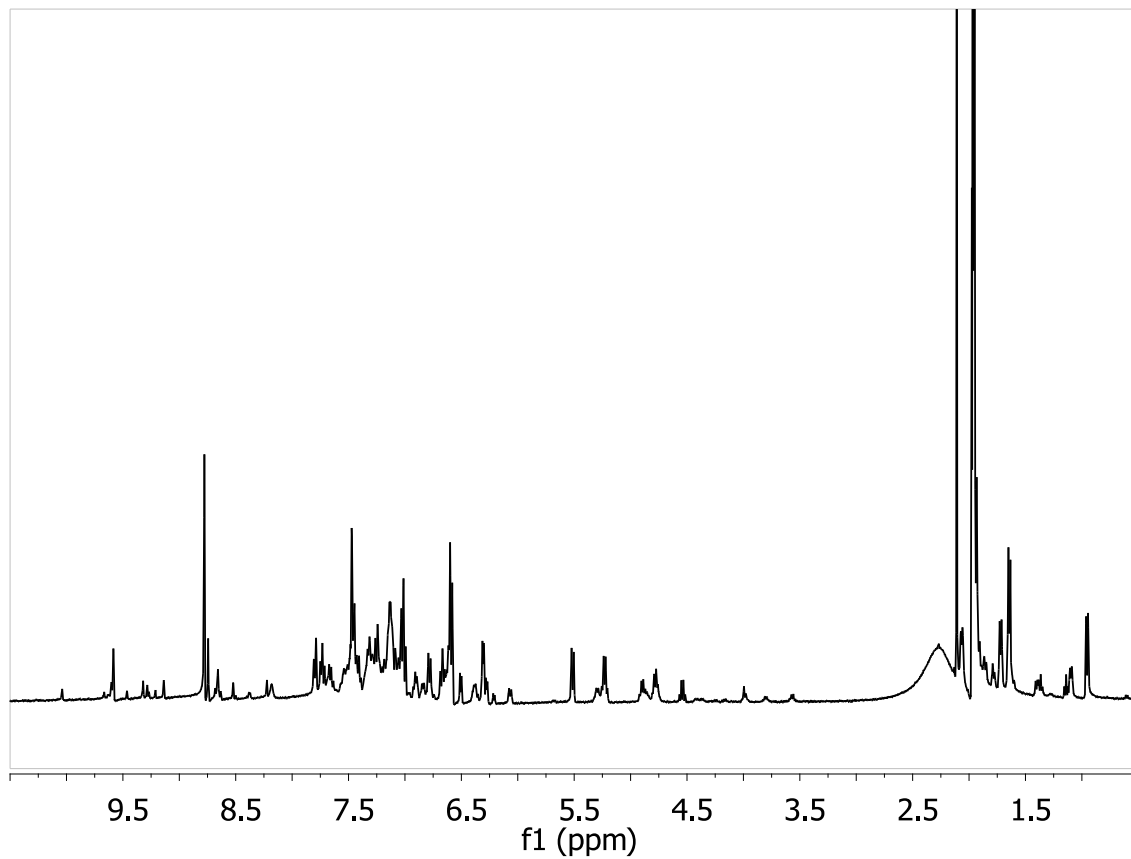


Figure S-10. The  $^1\text{H}$  NMR of the **MBI**-iron(II) complex at 20% *ee*.

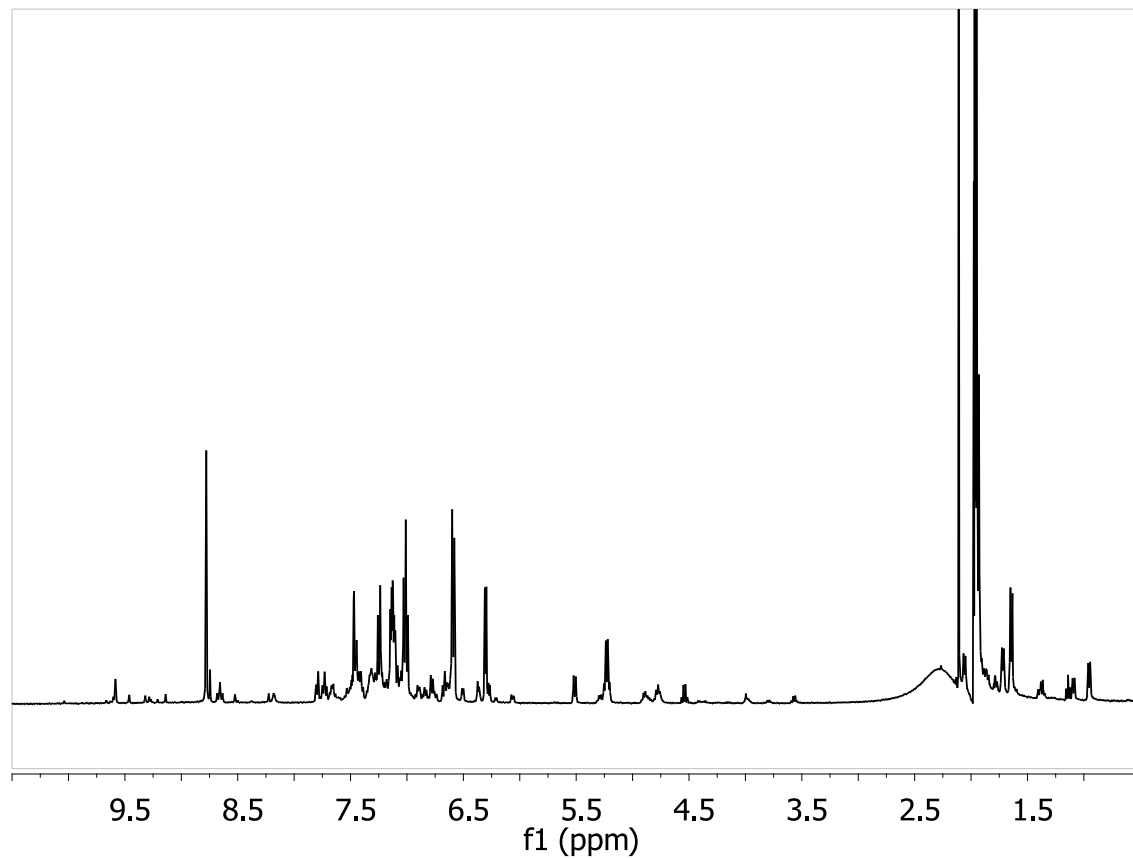


Figure S-11. The  $^1\text{H}$  NMR of the **MBI**-iron(II) complex at 60% *ee*.

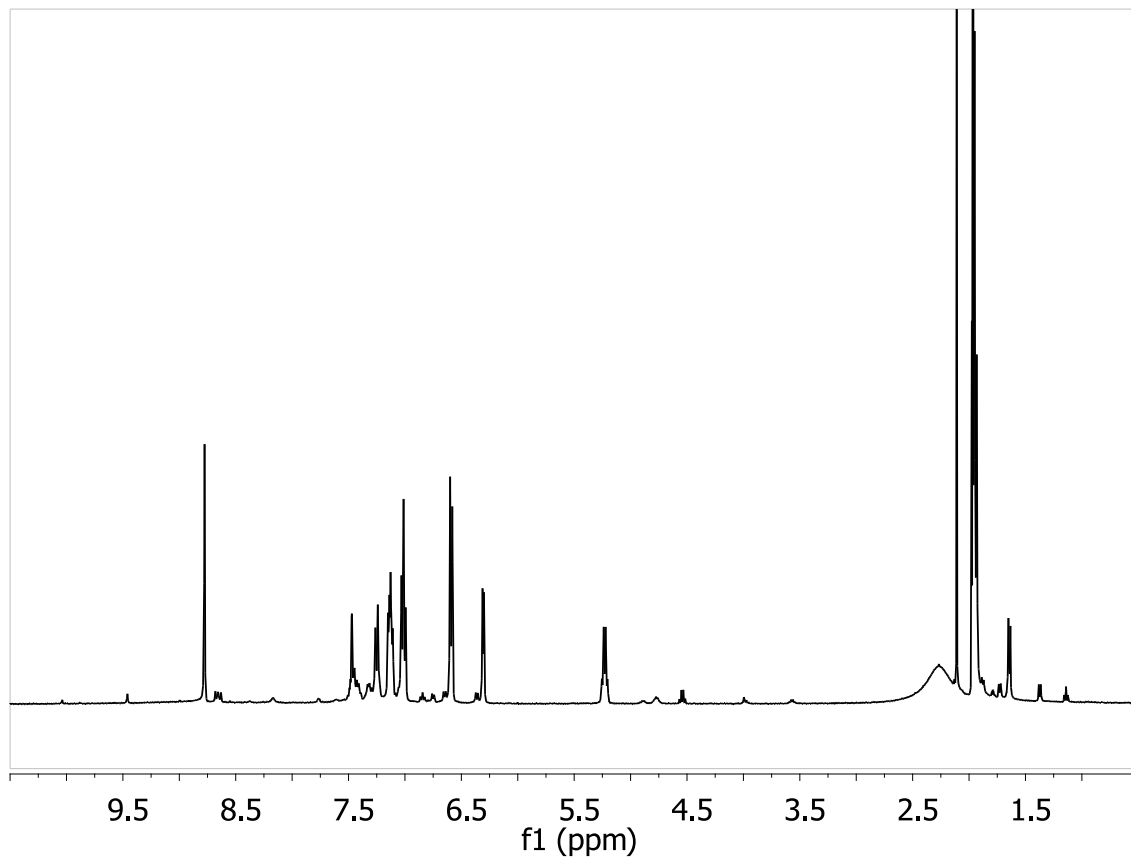


Figure S-12. The  $^1\text{H}$  NMR of the **MBI**-iron(II) complex at 100% *ee*.

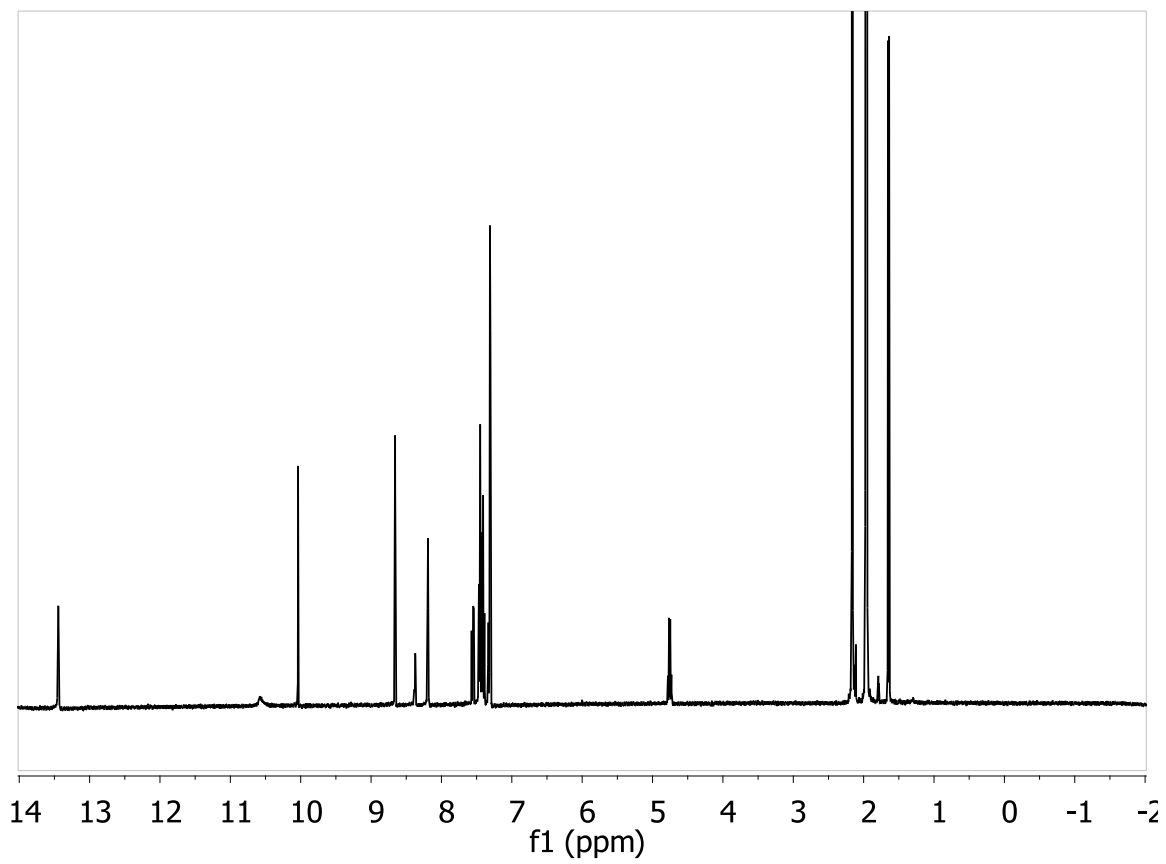


Figure S-13.  $^1\text{H}$  NMR of 10mM aldehyde **3** and 6mM **HPI**.



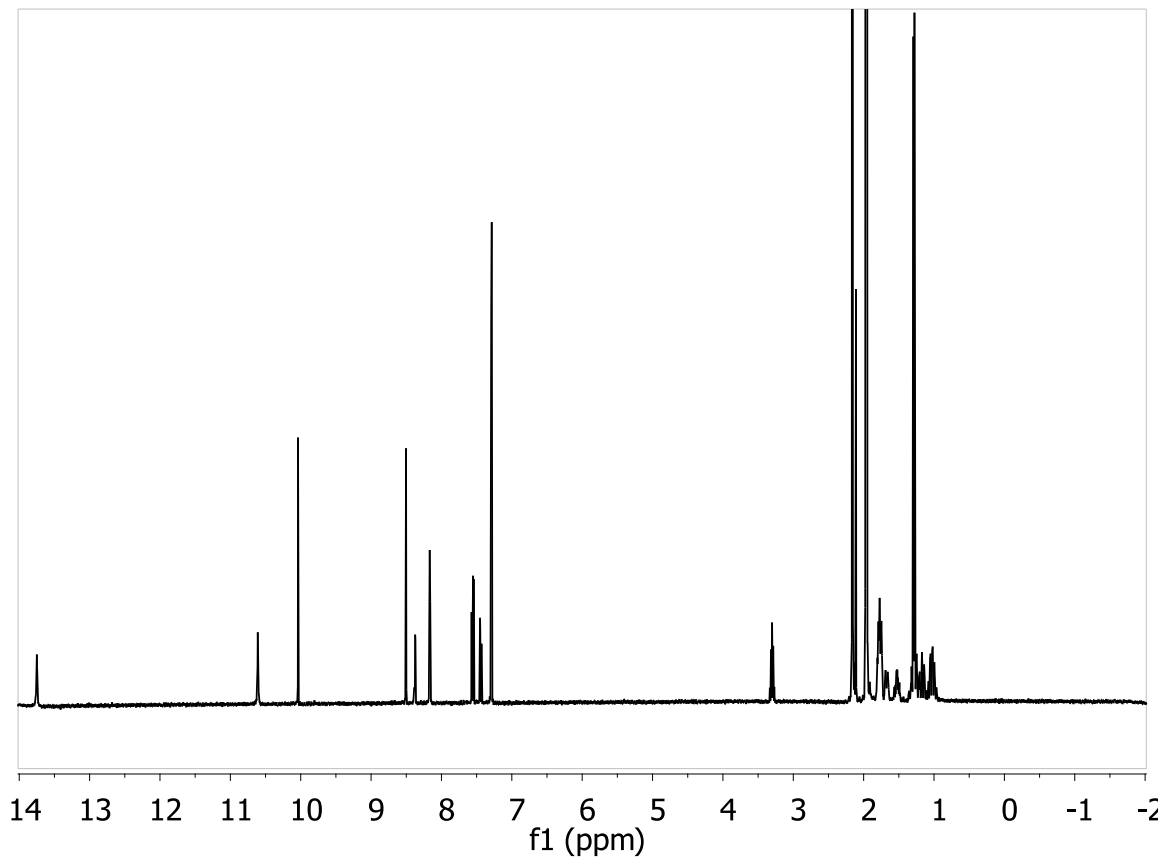


Figure S-14.  $^1\text{H}$  NMR of 10mM aldehyde **3** and 6mM of CEI.

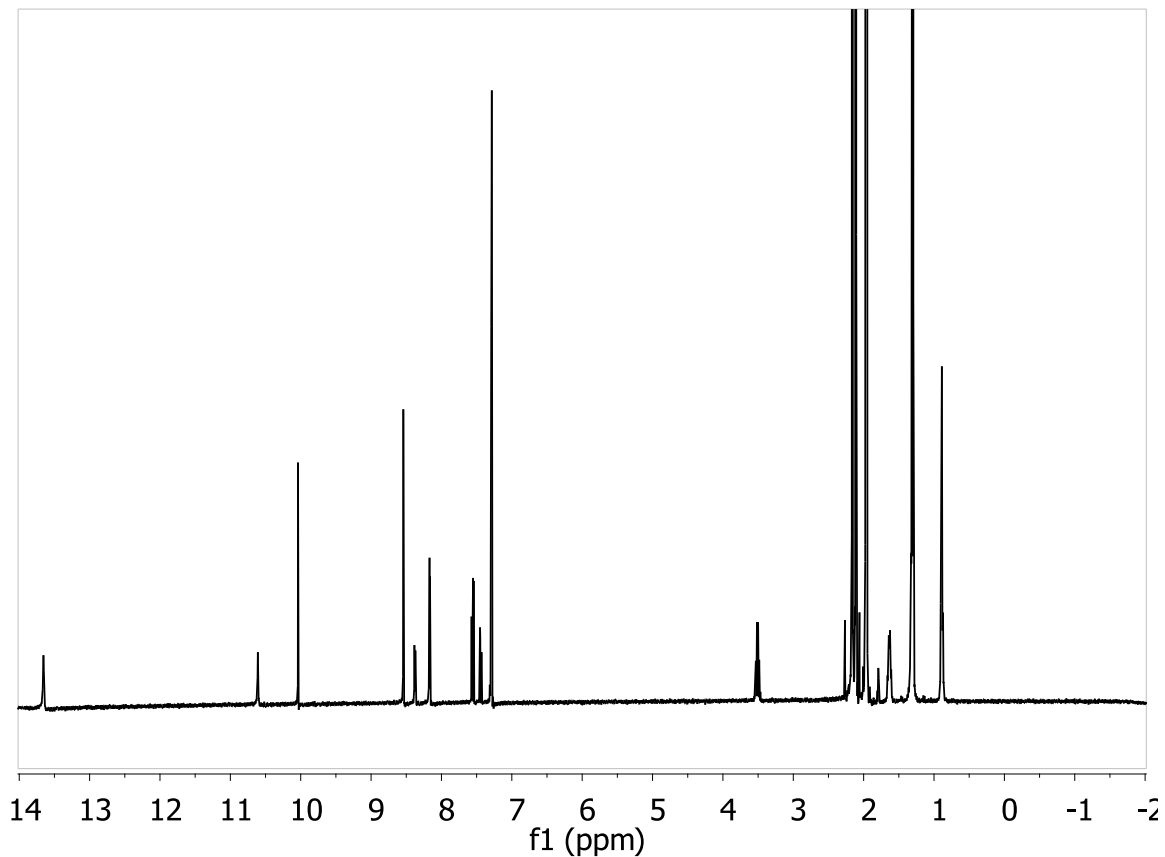


Figure S-15.  $^1\text{H}$  NMR of 10mM aldehyde **3** and 6mM **HPI**.

## VI. X-ray Crystallographic Data:

Table S-3. Crystal data and structure refinement for **1**.

Empirical formula	C <sub>47</sub> H <sub>50</sub> F <sub>6</sub> Fe N <sub>6.50</sub> O <sub>9.50</sub> S <sub>2</sub>	
Formula weight	1091.91	
Temperature	153(2) K	
Wavelength	0.71069 Å	
Crystal system	Orthorhombic	
Space group	P21212	
Unit cell dimensions	a = 30.495(2) Å	$\alpha = 90^\circ$ .
	b = 12.5164(9) Å	$\beta = 90^\circ$ .
	c = 13.3325(12) Å	$\gamma = 90^\circ$ .
Volume	5088.8(7) Å <sup>3</sup>	
Z	4	
Density (calculated)	1.425 Mg/m <sup>3</sup>	

Absorption coefficient	0.461 mm <sup>-1</sup>
F(000)	2262
Crystal size	0.45 x 0.32 x 0.04 mm
Theta range for data collection	1.67 to 25.03°.
Index ranges	-36<=h<=36, 0<=k<=14, 0<=l<=15
Reflections collected	8743
Independent reflections	8743
Completeness to theta = 25.03°	98.8 %
Absorption correction	Semi-empirical from equivalents
Max. and min. transmission	1.12 and 0.929
Refinement method	Full-matrix least-squares on F <sup>2</sup>
Data / restraints / parameters	8743 / 1050 / 790
Goodness-of-fit on F <sup>2</sup>	1.373
Final R indices [I>2sigma(I)]	R1 = 0.0948, wR2 = 0.1570
R indices (all data)	R1 = 0.1689, wR2 = 0.1752
Absolute structure parameter	0.00(3)
Largest diff. peak and hole	0.703 and -0.395 e.Å <sup>-3</sup>

Table S-4. Atomic coordinates ( $\times 10^4$ ) and equivalent isotropic displacement parameters ( $\text{\AA}^2 \times 10^3$ ) for 1.  $U(\text{eq})$  is defined as one third of the trace of the orthogonalized  $U^{ij}$  tensor.

	x	y	z	$U(\text{eq})$
Fe1	3142(1)	1649(1)	7490(1)	26(1)
O1	1628(2)	1159(4)	9089(3)	40(1)
O2	3281(2)	1136(4)	3626(3)	41(1)
O3	4534(2)	1068(5)	9532(4)	62(2)
N1	2600(2)	802(4)	7578(4)	21(1)
N2	2846(2)	2445(4)	8578(4)	24(1)
N3	2881(2)	2483(5)	6389(4)	29(2)
N4	3390(2)	835(4)	6352(4)	24(1)
N5	3458(2)	761(5)	8474(4)	28(2)
N6	3681(2)	2496(4)	7559(5)	29(1)
C1	2485(2)	-62(6)	7044(5)	30(2)
C2	2077(2)	-547(6)	7168(5)	35(2)
C3	1783(2)	-161(6)	7839(5)	33(2)
C4	1895(2)	720(6)	8406(5)	31(2)
C5	2303(2)	1172(5)	8247(5)	25(2)
C6	2469(2)	2095(5)	8791(5)	29(2)
C7	3036(2)	3366(6)	9183(5)	34(2)
C8	3327(2)	2899(6)	9986(5)	35(2)
C9	3210(3)	2039(6)	10577(5)	42(2)
C10	3484(3)	1663(7)	11309(6)	50(2)
C11	3875(3)	2084(7)	11482(6)	50(2)
C12	4007(3)	2943(8)	10945(7)	58(3)
C13	3732(3)	3340(7)	10201(6)	47(2)
C14	2686(2)	4086(6)	9660(5)	38(2)
C15	3681(2)	37(6)	6360(6)	34(2)
C16	3850(3)	-402(6)	5479(6)	40(2)
C17	3723(2)	-56(6)	4588(6)	35(2)
C18	3416(2)	763(6)	4549(5)	32(2)
C19	3264(2)	1215(5)	5437(5)	23(2)
C20	2972(2)	2120(6)	5517(6)	34(2)
C21	2573(2)	3382(6)	6469(5)	41(2)

C22	2107(3)	3007(6)	6641(5)	40(2)
C23	1923(3)	2242(6)	6036(6)	45(2)
C24	1491(3)	1940(8)	6160(7)	61(3)
C25	1226(3)	2422(7)	6882(7)	57(2)
C26	1414(3)	3201(7)	7493(7)	61(2)
C27	1857(3)	3502(6)	7377(6)	47(2)
C28	2587(3)	4128(6)	5572(5)	47(2)
C29	3333(3)	-150(6)	8893(5)	37(2)
C30	3607(3)	-735(7)	9551(6)	53(2)
C31	4007(3)	-332(8)	9793(6)	54(3)
C32	4144(3)	610(7)	9371(6)	41(2)
C33	3866(2)	1146(6)	8688(5)	32(2)
C34	3967(2)	2117(6)	8179(6)	38(2)
C35	3775(3)	3483(6)	6971(5)	40(2)
C36	3957(2)	3198(6)	5955(6)	39(2)
C37	4253(2)	2375(6)	5791(6)	44(2)
C38	4427(3)	2177(7)	4835(7)	57(3)
C39	4310(3)	2808(9)	4059(7)	68(3)
C40	4017(3)	3650(8)	4201(7)	63(3)
C41	3840(3)	3843(7)	5147(6)	47(2)
C42	4112(3)	4226(6)	7513(7)	66(3)
S1B	2731(1)	6800(2)	7553(3)	40(1)
F1B	3343(3)	6017(8)	6424(7)	60(4)
F2B	3560(3)	6484(10)	7890(7)	87(5)
F3B	3428(3)	7671(6)	6774(7)	80(3)
O1B	2497(4)	7074(11)	6645(8)	45(5)
O2B	2738(3)	7638(9)	8291(8)	41(4)
O3B	2645(4)	5749(6)	7934(9)	55(4)
C1B	3285(3)	6732(7)	7144(7)	68(4)
S1BA	2879(2)	6299(5)	6915(5)	45(2)
F1BA	3333(5)	8012(12)	7330(13)	68(5)
F2BA	3469(6)	6673(17)	8303(13)	63(6)
F3BA	2882(6)	7541(18)	8511(14)	50(6)
O1BA	2709(8)	5515(12)	7601(14)	44(6)
O2BA	3201(6)	5911(17)	6221(14)	59(8)
O3BA	2556(7)	7000(20)	6485(16)	44(9)

C1BA	3145(5)	7160(11)	7791(10)	58(6)
S1A	4521(1)	6549(3)	10892(3)	43(1)
F1A	4458(3)	6091(8)	8999(5)	88(3)
F2A	5071(3)	6762(8)	9409(6)	86(3)
F3A	4925(4)	5143(8)	9807(6)	104(4)
O1A	4192(4)	5741(10)	11083(10)	50(6)
O2A	4883(3)	6536(7)	11576(6)	53(3)
O3A	4346(3)	7585(6)	10669(7)	61(3)
C1A	4753(3)	6127(8)	9738(7)	83(5)
S1C	5130(1)	641(3)	11949(3)	40(1)
F1C	4861(2)	-69(8)	13680(4)	57(3)
F2C	4891(3)	-1257(5)	12535(7)	70(3)
F3C	4377(2)	-94(8)	12522(8)	69(3)
O1C	4958(3)	1676(5)	12228(7)	57(3)
O2C	5570(2)	440(9)	12255(8)	50(3)
O3C	5026(4)	318(6)	10940(4)	39(3)
C1C	4807(3)	-238(7)	12695(6)	61(3)
N1E	4240(7)	5677(16)	11419(19)	47(6)
C2E	4538(7)	5666(15)	11891(15)	57(5)
C3E	4897(5)	5725(13)	12516(15)	57(4)

---

Table S-5. Bond lengths [ $\text{\AA}$ ] and angles [ $^\circ$ ] for 1.

Fe1-N6	1.958(5)	C15-C16	1.395(10)
Fe1-N1	1.968(5)	C16-C17	1.323(9)
Fe1-N3	1.970(6)	C17-C18	1.388(10)
Fe1-N5	1.971(6)	C18-C19	1.392(9)
Fe1-N2	1.978(5)	C19-C20	1.443(9)
Fe1-N4	1.978(6)	C21-C28	1.517(9)
O1-C4	1.339(8)	C21-C22	1.515(10)
O2-C18	1.380(8)	C22-C23	1.372(10)
O3-C32	1.336(9)	C22-C27	1.388(10)
N1-C1	1.341(8)	C23-C24	1.379(11)
N1-C5	1.352(8)	C24-C25	1.394(11)
N2-C6	1.264(8)	C25-C26	1.394(12)
N2-C7	1.522(9)	C26-C27	1.413(11)
N3-C20	1.279(8)	C29-C30	1.416(10)
N3-C21	1.469(9)	C30-C31	1.359(11)
N4-C15	1.336(8)	C31-C32	1.372(12)
N4-C19	1.365(8)	C32-C33	1.415(10)
N5-C29	1.326(9)	C33-C34	1.426(10)
N5-C33	1.365(9)	C35-C36	1.507(10)
N6-C34	1.292(9)	C35-C42	1.562(10)
N6-C35	1.490(9)	C36-C37	1.387(10)
C1-C2	1.394(9)	C36-C41	1.394(11)
C2-C3	1.355(9)	C37-C38	1.402(10)
C3-C4	1.380(9)	C38-C39	1.350(12)
C4-C5	1.385(9)	C39-C40	1.394(12)
C5-C6	1.455(9)	C40-C41	1.393(11)
C7-C8	1.509(10)	S1B-O3B	1.434(6)
C7-C14	1.534(9)	S1B-O2B	1.438(6)
C8-C13	1.382(10)	S1B-O1B	1.446(6)
C8-C9	1.381(10)	S1B-C1B	1.778(9)
C9-C10	1.369(10)	F1B-C1B	1.325(8)
C10-C11	1.322(10)	F2B-C1B	1.338(8)
C11-C12	1.353(11)	F3B-C1B	1.347(8)
C12-C13	1.391(11)	S1BA-O2BA	1.433(7)

S1BA-O1BA	1.439(7)	F2A-C1A	1.328(8)
S1BA-O3BA	1.441(7)	F3A-C1A	1.343(8)
S1BA-C1BA	1.783(10)	S1C-O2C	1.424(6)
F1BA-C1BA	1.358(9)	S1C-O3C	1.440(6)
F2BA-C1BA	1.347(10)	S1C-O1C	1.446(6)
F3BA-C1BA	1.338(10)	S1C-C1C	1.779(9)
S1A-O2A	1.432(6)	F1C-C1C	1.340(8)
S1A-O3A	1.434(6)	F2C-C1C	1.318(8)
S1A-O1A	1.447(7)	F3C-C1C	1.344(8)
S1A-C1A	1.775(9)	N1E-C2E	1.11(3)
F1A-C1A	1.335(8)	C2E-C3E	1.38(2)
N6-Fe1-N1	173.9(3)	C15-N4-C19	117.1(6)
N6-Fe1-N3	95.1(2)	C15-N4-Fe1	129.3(5)
N1-Fe1-N3	89.4(2)	C19-N4-Fe1	113.5(4)
N6-Fe1-N5	82.2(2)	C29-N5-C33	118.6(6)
N1-Fe1-N5	93.8(2)	C29-N5-Fe1	128.7(5)
N3-Fe1-N5	173.1(2)	C33-N5-Fe1	112.7(5)
N6-Fe1-N2	94.4(2)	C34-N6-C35	120.7(6)
N1-Fe1-N2	81.0(2)	C34-N6-Fe1	113.4(5)
N3-Fe1-N2	95.5(2)	C35-N6-Fe1	125.9(5)
N5-Fe1-N2	91.1(2)	N1-C1-C2	121.4(6)
N6-Fe1-N4	89.6(2)	C3-C2-C1	120.9(7)
N1-Fe1-N4	95.1(2)	C2-C3-C4	118.9(7)
N3-Fe1-N4	81.7(2)	O1-C4-C3	123.4(6)
N5-Fe1-N4	91.9(2)	O1-C4-C5	118.9(6)
N2-Fe1-N4	175.3(2)	C3-C4-C5	117.6(6)
C1-N1-C5	116.9(6)	N1-C5-C4	124.3(6)
C1-N1-Fe1	128.5(5)	N1-C5-C6	111.7(6)
C5-N1-Fe1	114.6(4)	C4-C5-C6	124.0(6)
C6-N2-C7	119.3(6)	N2-C6-C5	118.6(6)
C6-N2-Fe1	114.0(5)	C8-C7-N2	107.8(6)
C7-N2-Fe1	126.7(4)	C8-C7-C14	110.0(6)
C20-N3-C21	118.5(6)	N2-C7-C14	113.6(5)
C20-N3-Fe1	113.6(5)	C13-C8-C9	115.1(8)
C21-N3-Fe1	127.6(4)	C13-C8-C7	121.2(7)



C9-C8-C7	123.7(7)	N6-C34-C33	118.2(7)
C10-C9-C8	121.1(8)	N6-C35-C36	110.3(6)
C11-C10-C9	122.6(9)	N6-C35-C42	112.2(6)
C10-C11-C12	119.5(8)	C36-C35-C42	108.3(6)
C11-C12-C13	118.8(8)	C37-C36-C41	118.4(7)
C8-C13-C12	123.0(9)	C37-C36-C35	123.9(7)
N4-C15-C16	122.3(7)	C41-C36-C35	117.6(7)
C17-C16-C15	121.2(7)	C36-C37-C38	121.4(8)
C16-C17-C18	118.3(7)	C39-C38-C37	119.6(9)
O2-C18-C17	119.0(6)	C38-C39-C40	120.4(9)
O2-C18-C19	121.4(6)	C41-C40-C39	120.3(9)
C17-C18-C19	119.6(6)	C40-C41-C36	120.0(8)
N4-C19-C18	121.6(6)	O3B-S1B-O2B	115.5(5)
N4-C19-C20	112.4(6)	O3B-S1B-O1B	115.1(5)
C18-C19-C20	126.0(6)	O2B-S1B-O1B	114.0(5)
N3-C20-C19	118.7(7)	O3B-S1B-C1B	103.8(5)
N3-C21-C28	113.4(6)	O2B-S1B-C1B	103.2(4)
N3-C21-C22	111.9(6)	O1B-S1B-C1B	102.9(5)
C28-C21-C22	109.7(6)	F1B-C1B-F2B	107.3(7)
C23-C22-C27	120.2(8)	F1B-C1B-F3B	106.3(7)
C23-C22-C21	120.8(7)	F2B-C1B-F3B	105.8(7)
C27-C22-C21	118.9(8)	F1B-C1B-S1B	112.5(6)
C22-C23-C24	120.7(8)	F2B-C1B-S1B	112.3(6)
C23-C24-C25	121.2(9)	F3B-C1B-S1B	112.2(6)
C24-C25-C26	117.9(9)	O2BA-S1BA-O1BA	115.2(7)
C25-C26-C27	121.0(8)	O2BA-S1BA-O3BA	114.7(7)
C22-C27-C26	119.0(8)	O1BA-S1BA-O3BA	115.0(7)
N5-C29-C30	122.4(7)	O2BA-S1BA-C1BA	108.5(12)
C31-C30-C29	119.0(8)	O1BA-S1BA-C1BA	99.2(10)
C30-C31-C32	119.8(8)	O3BA-S1BA-C1BA	101.7(13)
O3-C32-C31	125.1(8)	F3BA-C1BA-F2BA	103.7(15)
O3-C32-C33	115.7(8)	F3BA-C1BA-F1BA	107.4(17)
C31-C32-C33	119.2(8)	F2BA-C1BA-F1BA	106.0(16)
N5-C33-C32	121.0(7)	F3BA-C1BA-S1BA	114.4(12)
N5-C33-C34	113.5(7)	F2BA-C1BA-S1BA	113.0(11)
C32-C33-C34	125.5(7)	F1BA-C1BA-S1BA	111.7(11)

O2A-S1A-O3A	115.5(5)
O2A-S1A-O1A	114.5(5)
O3A-S1A-O1A	114.2(5)
O2A-S1A-C1A	104.0(4)
O3A-S1A-C1A	103.7(4)
O1A-S1A-C1A	102.8(5)
F2A-C1A-F1A	105.7(7)
F2A-C1A-F3A	106.7(7)
F1A-C1A-F3A	106.5(7)
F2A-C1A-S1A	113.6(6)
F1A-C1A-S1A	112.3(6)
F3A-C1A-S1A	111.7(6)
O2C-S1C-O3C	115.1(5)
O2C-S1C-O1C	115.3(5)
O3C-S1C-O1C	114.3(5)
O2C-S1C-C1C	104.5(4)
O3C-S1C-C1C	103.1(4)
O1C-S1C-C1C	102.1(4)
F2C-C1C-F1C	106.7(7)
F2C-C1C-F3C	106.9(7)
F1C-C1C-F3C	105.5(7)
F2C-C1C-S1C	113.6(6)
F1C-C1C-S1C	112.5(6)
F3C-C1C-S1C	111.1(6)
N1E-C2E-C3E	175(2)

Table S-6. Anisotropic displacement parameters ( $\text{\AA}^2 \times 10^3$ ) for 1. The anisotropic displacement factor exponent takes the form:  $-2\pi^2 [ h^2 a^{*2} U^{11} + \dots + 2 h k a^* b^* U^{12} ]$

	U <sup>11</sup>	U <sup>22</sup>	U <sup>33</sup>	U <sup>23</sup>	U <sup>13</sup>	U <sup>12</sup>
Fe1	33(1)	24(1)	21(1)	0(1)	1(1)	2(1)
O1	50(3)	44(3)	26(3)	-6(3)	7(3)	2(3)
O2	51(3)	50(3)	21(3)	1(3)	7(3)	-3(3)
O3	41(4)	98(5)	48(4)	-16(3)	-18(3)	4(3)
N1	33(3)	16(3)	15(3)	1(3)	1(3)	4(2)
N2	28(3)	25(3)	20(3)	-5(3)	5(3)	4(3)
N3	41(4)	32(4)	14(3)	-4(3)	11(3)	6(3)
N4	24(3)	26(4)	22(3)	5(3)	3(3)	4(3)
N5	38(4)	28(4)	18(3)	-2(3)	8(3)	-6(3)
N6	28(3)	24(3)	33(3)	-1(3)	0(3)	0(2)
C1	37(4)	25(4)	28(4)	11(3)	4(3)	9(3)
C2	35(4)	37(4)	34(5)	-8(3)	-4(4)	-6(4)
C3	34(4)	38(4)	28(4)	4(3)	-5(3)	-9(3)
C4	31(4)	42(4)	18(4)	5(3)	5(3)	-2(4)
C5	24(4)	31(4)	20(4)	3(3)	2(3)	6(3)
C6	33(4)	31(4)	24(4)	2(3)	6(3)	5(3)
C7	42(4)	30(4)	29(4)	-4(4)	-1(3)	-3(4)
C8	34(4)	47(5)	24(4)	-13(4)	8(3)	1(4)
C9	56(5)	50(5)	22(4)	-4(4)	4(4)	-1(4)
C10	56(5)	64(5)	31(4)	-5(4)	-4(4)	10(5)
C11	51(5)	68(6)	30(4)	-13(4)	-13(4)	10(4)
C12	51(5)	72(6)	50(5)	-26(5)	-15(5)	3(5)
C13	41(4)	56(5)	44(5)	-22(4)	5(4)	7(4)
C14	54(5)	29(5)	30(4)	-23(4)	6(4)	5(4)
C15	37(4)	36(4)	28(4)	-2(4)	-3(4)	0(4)
C16	43(5)	33(5)	44(5)	-13(4)	9(4)	9(4)
C17	40(4)	40(4)	24(4)	-5(4)	0(4)	6(4)
C18	38(4)	35(4)	22(4)	4(4)	-2(4)	-7(4)
C19	16(4)	27(4)	25(4)	-2(3)	4(3)	-2(3)
C20	38(4)	37(4)	27(4)	6(4)	1(3)	1(4)
C21	52(5)	35(4)	35(4)	11(4)	4(4)	15(4)

C22	57(5)	43(5)	19(4)	10(4)	7(4)	19(4)
C23	45(5)	50(5)	41(5)	9(4)	8(4)	18(4)
C24	60(5)	66(6)	58(5)	13(5)	-2(5)	8(5)
C25	51(5)	74(6)	48(5)	27(5)	4(4)	14(5)
C26	65(5)	79(5)	39(4)	9(5)	14(5)	34(4)
C27	53(4)	56(5)	32(4)	10(4)	-2(4)	23(4)
C28	75(6)	32(5)	34(5)	11(4)	18(4)	20(4)
C29	47(4)	38(5)	26(4)	4(4)	-1(4)	6(4)
C30	78(6)	46(5)	35(5)	12(4)	4(5)	10(5)
C31	44(5)	69(6)	49(5)	2(5)	-5(4)	25(5)
C32	39(5)	56(5)	27(4)	-14(4)	-6(4)	17(4)
C33	35(4)	39(4)	22(4)	-4(4)	0(3)	0(4)
C34	29(4)	43(5)	40(4)	-20(4)	1(4)	5(4)
C35	53(5)	25(4)	42(4)	-5(4)	18(4)	-8(4)
C36	44(4)	30(4)	44(5)	-11(4)	8(4)	-21(4)
C37	50(5)	34(5)	49(5)	3(4)	23(4)	-8(4)
C38	56(5)	56(5)	58(5)	-10(5)	20(5)	-10(4)
C39	67(6)	85(6)	51(5)	-32(5)	4(5)	-14(5)
C40	45(5)	86(6)	56(6)	6(5)	-11(4)	-14(5)
C41	45(5)	55(5)	42(5)	-3(4)	9(4)	-1(4)
C42	93(6)	50(5)	54(5)	-10(6)	18(6)	-41(5)
S1B	42(2)	38(2)	39(2)	5(2)	-2(2)	-7(1)
F1B	66(6)	57(6)	57(6)	-42(5)	13(6)	-3(5)
F2B	73(7)	110(9)	78(9)	-26(7)	-14(6)	29(6)
F3B	93(7)	57(6)	91(8)	-6(6)	30(6)	-33(5)
O1B	51(8)	42(8)	43(8)	6(6)	-12(7)	-11(6)
O2B	49(8)	39(6)	35(7)	-17(5)	-8(6)	6(6)
O3B	79(8)	41(7)	45(8)	9(6)	11(6)	-17(6)
C1B	73(8)	64(7)	67(8)	-15(7)	-1(7)	-4(7)
S1BA	51(4)	42(4)	40(3)	-6(3)	3(3)	7(3)
F1BA	76(9)	59(9)	70(10)	7(9)	-6(9)	-27(7)
F2BA	54(9)	80(11)	55(10)	-27(9)	-32(8)	20(8)
F3BA	48(10)	57(10)	45(10)	-21(8)	-15(9)	7(8)
O1BA	69(11)	29(9)	33(11)	-6(9)	3(10)	-11(8)
O2BA	76(14)	47(12)	54(12)	-17(9)	-14(11)	10(10)
O3BA	47(13)	51(15)	35(12)	3(10)	-4(10)	17(11)

C1BA	53(9)	58(9)	63(10)	4(8)	-3(8)	-5(8)
S1A	42(2)	43(3)	44(2)	6(2)	8(2)	-1(2)
F1A	81(7)	130(8)	52(6)	-29(6)	-17(6)	4(6)
F2A	84(7)	95(7)	80(7)	-13(6)	38(6)	-27(6)
F3A	114(10)	105(8)	93(6)	-22(9)	39(8)	25(7)
O1A	45(9)	55(9)	50(10)	5(7)	0(7)	1(7)
O2A	42(6)	58(7)	58(7)	2(6)	-14(5)	-14(6)
O3A	60(7)	41(7)	84(8)	21(6)	4(6)	15(6)
C1A	84(8)	90(8)	75(8)	-11(7)	13(7)	0(7)
S1C	35(2)	48(3)	36(2)	-10(2)	2(2)	0(2)
F1C	66(7)	64(5)	40(4)	-5(5)	16(4)	5(6)
F2C	85(6)	60(5)	64(5)	-7(5)	18(5)	3(5)
F3C	67(5)	65(6)	74(6)	-1(6)	7(5)	-10(5)
O1C	59(6)	55(6)	56(6)	-15(5)	1(5)	4(5)
O2C	38(5)	64(6)	49(6)	5(5)	-3(5)	-2(5)
O3C	40(5)	48(7)	30(4)	1(4)	-4(5)	7(6)
C1C	66(6)	57(5)	58(5)	-7(5)	6(5)	0(5)
N1E	44(11)	40(10)	57(12)	-13(8)	7(9)	1(9)
C2E	56(8)	55(8)	59(9)	-3(7)	-5(8)	1(7)
C3E	52(7)	66(8)	54(8)	-6(8)	-2(8)	3(7)

---

Table S-7. Hydrogen coordinates ( $\times 10^4$ ) and isotropic displacement parameters ( $\text{\AA}^2 \times 10^{-3}$ ) for 1.

	x	y	z	U(eq)
H1O	1778	1455	9538	60
H2O	3500	1333	3293	61
H3O	4646	813	10055	94
H1	2686	-350	6571	36
H2	2004	-1155	6776	42
H3	1505	-492	7917	40
H6	2297	2428	9296	35
H7	3221	3813	8728	40
H9	2934	1703	10474	51
H10	3390	1077	11708	60
H11	4061	1785	11980	59
H12	4282	3269	11075	69
H13	3827	3940	9824	56
H14A	2469	4286	9152	56
H14B	2825	4732	9927	56
H14C	2541	3700	10206	56
H15	3776	-241	6986	41
H16	4061	-959	5520	48
H17	3838	-360	3990	42
H20	2851	2440	4933	41
H21	2661	3808	7070	49
H23	2094	1918	5525	54
H24	1373	1394	5747	73
H25	927	2226	6954	69
H26	1241	3535	7997	74
H27	1982	4036	7795	56
H28A	2893	4290	5405	70
H28B	2432	4792	5735	70
H28C	2445	3784	4997	70
H29	3049	-419	8747	44

H30	3512	-1400	9819	63
H31	4190	-701	10252	65
H34	4237	2476	8293	45
H35	3495	3886	6876	48
H37	4340	1937	6338	53
H38	4625	1602	4734	68
H39	4429	2679	3411	81
H40	3938	4093	3652	75
H41	3639	4414	5240	57
H42A	4019	4339	8208	98
H42B	4126	4915	7165	98
H42C	4402	3890	7505	98

## VII. Computational Details:

Molecular mechanics calculations were run with Spartan'10 (Wavefunction, Inc., Irvine, CA) with defaults grids and convergence criteria. Density functional theory (DFT), time-dependent DFT (TDDFT) calculations and ZINDO calculations were run with Gaussian '09<sup>1</sup> with default grids and convergence criteria.

The starting geometry for the calculations was obtained from the X-ray structure of *S-MBI- $\Delta$ -fac* Fe(II) complex, which was edited to obtain all possible isomers of (*S-S-S*)-**MBI**-Fe(II) complex. A conformational search was run on these structures using Merck Molecular force field (MMFF) and the Monte Carlo algorithm implemented in Spartan'10. All MMFF minima were then optimized with DFT using BPV86 functional, which consists of Becke's 1986 exchange functional and Becke-Perdew correlation functional with Vosko-Wilk-Nusair local density approximation.<sup>2</sup> Other functionals were also tested, including: B3LYP; LC-BPV86, where BPV86 is modified with Hirao's long-range correction; Truhlar and Zhao's M06-2X.<sup>2</sup> The basis set was the triple- $\zeta$  Ahlrich's TZVP set for H, C, N and O, and LanL2DZ basis set for Fe which

consists of a double- $\zeta$  basis and a Los Alamos effective core potential (ECP).<sup>3</sup> In some cases, the Polarizable Continuum solvent Model (PCM) for acetonitrile was used.<sup>4</sup>

CD calculations were run using both ZINDO method and TDDFT method, at the same level of calculation employed for the geometry optimizations [BPV86/TZVP+Lan2DZ(Fe)]. ECD spectra were generated using the program SpecDis (v. 1.50, T. Bruhn, V. Hemberger, A. Schaumlöffel, G. Bringmann, Univ. Würzburg, Germany, 2010) by applying a Gaussian band shape with 0.22 eV exponential half-width, from dipole-length rotational strengths; the difference from dipole-velocity values was negligible (<10%) for most transitions.

The model ligand 2-((methylimino)methyl)pyridin-3-ol (**MIP**) was optimized at B3LYP/6-31G(d) and resulting geometry had Cs symmetry. Excited-state calculations were run on **MIP** with ZINDO and TDDFT method at CAM-B3LYP/SVP level.<sup>2,3</sup>



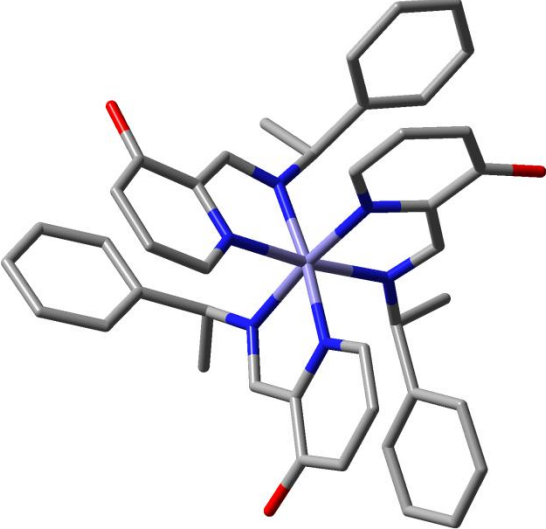
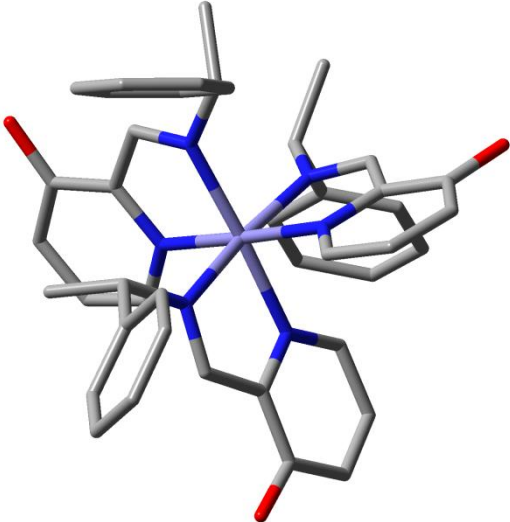
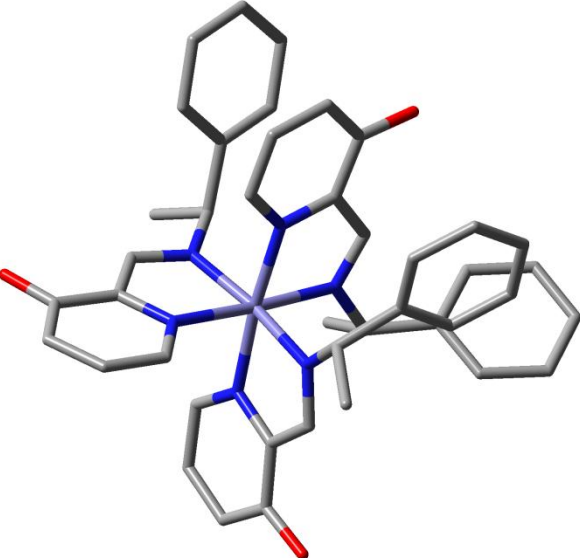
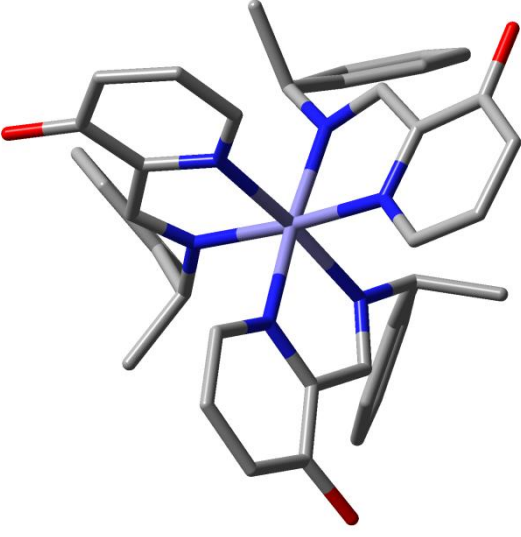
	
<p><math>\Delta</math>-<i>fac</i> (global minimum)</p>	<p><math>\Lambda</math>-<i>mer</i> (+0.57 kcal/mol)</p>
	
<p><math>\Delta</math>-<i>mer</i> (+3.46 kcal/mol)</p>	<p><math>\Lambda</math>-<i>fac</i> (+7.08 kcal/mol)</p>

Table S-8. DFT-optimized structures for (*S,S,S*)-**MBI**-Fe(II) complex at BPV86/TZVP+ LanL2DZ(Fe) level, with relative internal energies. The lowest-energy conformer is shown for each diastereomer. Hydrogen atoms omitted for clarity.

## References:

(1) Frisch, M. J.; Trucks, G. W.; Schlegel, H. B.; Scuseria, G. E.; Robb, M. A.; Cheeseman, J. R.; Scalmani, G.; Barone, V.; Mennucci, B.; Petersson, G. A.; Nakatsuji, H.; Caricato, M.; Li, X.; Hratchian, H. P.; Izmaylov, A. F.; Bloino, J.; Zheng, G.; Sonnenberg, J. L.; Hada, M.; Ehara, M.; Toyota, K.; Fukuda, R.; Hasegawa, J.; Ishida, M.; Nakajima, T.; Honda, Y.; Kitao, O.; Nakai, H.; Vreven, T.; Montgomery, J. A.; Peralta, J. E.; Ogliaro, F.; Bearpark, M.; Heyd, J. J.; Brothers, E.; Kudin, K. N.; Staroverov, V. N.; Kobayashi, R.; Normand, J.; Raghavachari, K.; Rendell, A.; Burant, J. C.; Iyengar, S. S.; Tomasi, J.; Cossi, M.; Rega, N.; Millam, J. M.; Klene, M.; Knox, J. E.; Cross, J. B.; Bakken, V.; Adamo, C.; Jaramillo, J.; Gomperts, R.; Stratmann, R. E.; Yazyev, O.; Austin, A. J.; Cammi, R.; Pomelli, C.; Ochterski, J. W.; Martin, R. L.; Morokuma, K.; Zakrzewski, V. G.; Voth, G. A.; Salvador, P.; Dannenberg, J. J.; Dapprich, S.; Daniels, A. D.; Farkas; Foresman, J. B.; Ortiz, J. V.; Cioslowski, J.; Fox, D. J. Wallingford CT, 2009.

(2) All references about DFT functionals can be found in the on-line documentation for Gaussian'09 at [http://www.gaussian.com/g\\_tech/g\\_ur/k\\_dft.htm](http://www.gaussian.com/g_tech/g_ur/k_dft.htm).

(3) All references about basis sets can be found in the on-line documentation for Gaussian'09 at [http://www.gaussian.com/g\\_tech/g\\_ur/m\\_basis\\_sets.htm](http://www.gaussian.com/g_tech/g_ur/m_basis_sets.htm).

(4) *Continuum Solvation Models in Chemical Physics: From Theory to Applications* Mennucci, B.; Cammi, R., Eds.; Wiley: Chichester, 2007.